NDT Advance Access published September 15, 2013

Nephrol Dial Transplant (2013) 0: 1–8
doi: 10.1093/ndt/gft359

Original Article

LMX1B mutation with residual transcriptional activity as a cause of isolated glomerulopathy

Tsuyoshi Isojima[1], Yutaka Harita[1], Masayuki Furuyama[2], Noriko Sugawara[2], Kiyonobu Ishizuka[2], Shigeru Horita[2], Yuko Kajiho[1], Kenichiro Miura[1], Takashi Igarashi[1], Motoshi Hattori[2] and Sachiko Kitanaka[1]

[1]Department of Pediatrics, Graduate School of Medicine, The University of Tokyo, Bunkyo-ku, Tokyo, Japan and [2]Department of Pediatric Nephrology, Tokyo Women's Medical College, Shinjuku-ku, Tokyo, Japan

Correspondence and offprint requests to: Sachiko Kitanaka; E-mail: sachi-tky@umin.ac.jp

Keywords: glomerulopathy, LMX1B, nail–patella like renal disease, podocyte

ABSTRACT

Background. Nail–patella syndrome (NPS) is a rare autosomal-dominant disorder caused by *LMX1B* mutation. In patients with the renal lesions typical of NPS without skeletal or nail findings, it is described as nail–patella-like renal disease (NPLRD). However, the pathogenesis of NPLRD is largely unknown.

Methods. A 6-year-old girl with microscopic haematuria and mild proteinuria was diagnosed with NPLRD because of an aberrantly thickened glomerular basement membrane (GBM) and deposition of Type III collagen in the GBM observed by electron microscopy. Immunohistological analyses of podocyte protein expression were performed on biopsy tissues. Sequence analysis of *LMX1B* was performed, and the functional consequences of the detected mutation were analysed by luciferase reporter assay.

Results. When analysing molecules that are important for podocyte development, maintenance and maturation, CD2AP expression was found to be altered in the podocytes. A novel *LMX1B* missense mutation (R246Q) was identified. Functional analyses revealed partial but significant impairment of R246Q transcriptional activity. However, no dominant-negative effect of R246Q was detected, which suggests that NPLRD is caused by LMX1B haploinsufficiency.

Conclusions. This is the first report on *LMX1B* mutation identified in a patient with NPLRD. Residual transcriptional activity would account for normality of the nails and patella in this case. Genetic and pathological analyses of additional cases would clarify the role of *LMX1B* in glomerulopathy without systemic symptoms, which, together with nephropathy in NPS, can be designated as 'LMX1B nephropathy'.

INTRODUCTION

Nail–patella syndrome (NPS; OMIM #161200) is a rare autosomal-dominant disease characterized by dysplastic nails, absent or hypoplastic patellae, elbow dysplasia, iliac horns

and, in some cases, open-angle glaucoma and nephropathy [1–3]. It is caused by heterozygous mutations in the LIM homeodomain transcription factor *LMX1B* [4–6], which plays a fundamental role in pattern formation during vertebrate limb development and kidney morphogenesis [5–7]. Most of the patients with NPS have skeletal (90%) and/or nail (98%) phenotypes [3]. However, nephropathy has been reported in ~40% of affected individuals [7]. The severity of nephropathy is extremely variable both within and between families. Since nephropathy rapidly progresses during early childhood in some patients [8], NPS diagnosis during childhood is desirable. The characteristic histological changes of NPS nephropathy consist of irregular thickening of the glomerular basement membrane (GBM) with electron-lucent areas containing bundles of Type III collagen observed by electron microscopy [8]. While Lmx1b is exclusively expressed in the glomeruli of mouse kidney, and podocyte-specific knockout of *Lmx1b* in mice causes foot process effacement [9], its role in human podocytes *in vivo* is still largely unknown [10].

Cases with the renal lesions typical of NPS without the skeletal and nail findings have also been reported [7, 11, 12]. In these cases, the condition is known as nail–patella-like renal disease (NPLRD; OMIM #256020). To date, since very few cases have been reported, NPLRD pathogenesis remains unknown; in these patients, NPLRD may represent the partial expression of NPS or an independent genetic form of glomerular membrane disease [7, 11, 12]. Therefore, genetic analysis of *LMX1B* for these patients is vital to reveal the pathogenesis of this extremely rare entity.

Here, we describe the case of a patient with microscopic haematuria and mild proteinuria diagnosed as NPLRD by electron microscopy in which a novel *LMX1B* mutation was identified. Functional analyses of the mutant protein showed partially impaired transcriptional activity. This is the first report identifying the responsible gene mutation in a patient with NPLRD. Further pathological and genetic analyses will unveil the prevalence and morbidity of 'LMX1B nephropathy' in patients with NPS and with other minor urinary abnormalities.

MATERIALS AND METHODS

Materials

Tissue for light microscopy was collected and processed routinely. Tissue for direct immunofluorescence was stained utilizing fluorescein-tagged antibodies against IgA, IgG, IgM, C3 complement, C4d, C1q complement and fibrinogen. Biopsy tissue for electron microscopy was routinely fixed, and some sections were also prestained with tannic acid to highlight collagen. In addition, the α2 chain of Type IV collagen, α5 chain of Type IV collagen and Type III collagen were stained with FITC-anti-collagen IV α2 (IV) human (mono) (Shigei Medical Research Institute, Okayama, Japan), Texas Red-anti-collagen IV α5 (IV) human (mono) (Shigei Medical Research Institute) and goat anti-Type III collagen (Southern Biotechnology Associates, Inc., Birmingham, AL, USA), respectively. Immunohistological analysis of podocyte protein expression was performed. Paraffin-embedded samples from human renal biopsy samples were deparaffinized in xylene and rehydrated through graded alcohols in H_2O, followed by heat-induced epitope retrieval by incubating in a target retrieval solution (S1699; Dako, Carpinteria, CA, USA) for 15 min at 121° C. Sections were cooled to room temperature and incubated with the primary antibodies, followed by incubation with Alexa Fluor-conjugated secondary antibodies (Invitrogen, Carlsbad, CA, USA). Images were obtained using an inverted microscope (model IX71; Olympus, Tokyo, Japan) and processed using Adobe Photoshop CS3. The following antibodies were commercially obtained: mouse monoclonal anti-ZO-1 IgG (33-9100; Invitrogen), mouse monoclonal anti-GLEPP-1 IgG (MU336-UC; BioGenex, San Ramon, CA, USA), mouse monoclonal anti-WT1 IgG (M3561; Dako), rabbit polyclonal anti-synaptopodin (Meridian Life Science, Memphis, TN, USA), mouse monoclonal anti-vimentin (Dako), rabbit polyclonal anti-CD2AP (Sigma, St. Louis, MO, USA) and mouse monoclonal anti-ezrin (Sigma). Rabbit polyclonal anti-nephrin IgG and rabbit polyclonal anti-podocin were previously described [13, 14]. Normal control samples (donor kidney) were stained simultaneously.

LMX1B gene analysis

Informed consent for DNA analysis was obtained from the patient and her parents. The study was performed with the approval of the Ethics Committee of The University of Tokyo. Genomic DNA was extracted from peripheral white blood cells of the patient and her parents using a QIAamp DNA Blood Midi Kit (Qiagen, Hilden, Germany). The entire coding region and exon–intron boundaries of *LMX1B* were amplified from the genomic DNA by polymerase chain reaction (PCR). The primers used for PCR amplification and PCR conditions were previously described [15]. Subsequently, PCR products were sequenced using an ABI Prism BigDye Terminator Cycle Sequencing Ready Reaction Kit (PE Applied Biosystems, Foster City, CA, USA) and the forward and reverse primers from PCR amplification. Direct sequencing in both directions was performed on an autosequencer (ABI PRISM 310 Genetic Analyzer; Applied Biosystems). Specimens from a population of 50 healthy Japanese control subjects with no symptoms were similarly analysed to show that the missense mutation identified in the patient was not a variant.

Plasmid construction

The constructs of wild-type LMX1B expression plasmid LMX1B-pcDNA3.1, shPan1 expression plasmid shPan1-BAT14 and luciferase reporter plasmid 5xFar/FLAT-pFOXluc1.prl that contained five copies of the rat insulin mini-enhancer element E2A3/4(Far/FLAT) have been previously described [16–18]. Mutant plasmids LMX1B-R246Q and LMX1B-V265L were created using a Quick Change Site-directed Mutagenesis Kit (Stratagene, La Jolla, CA, USA) according to the manufacturer's protocol [15]. The mutant constructs were sequence-verified to ensure that there were no extra mutations.

Cell culture and transfection

The transcriptional activity of LMX1B was analysed as previously reported [15]. In brief, Cos-1 cells were maintained in Dulbecco's Modified Eagle Medium supplemented with 10%

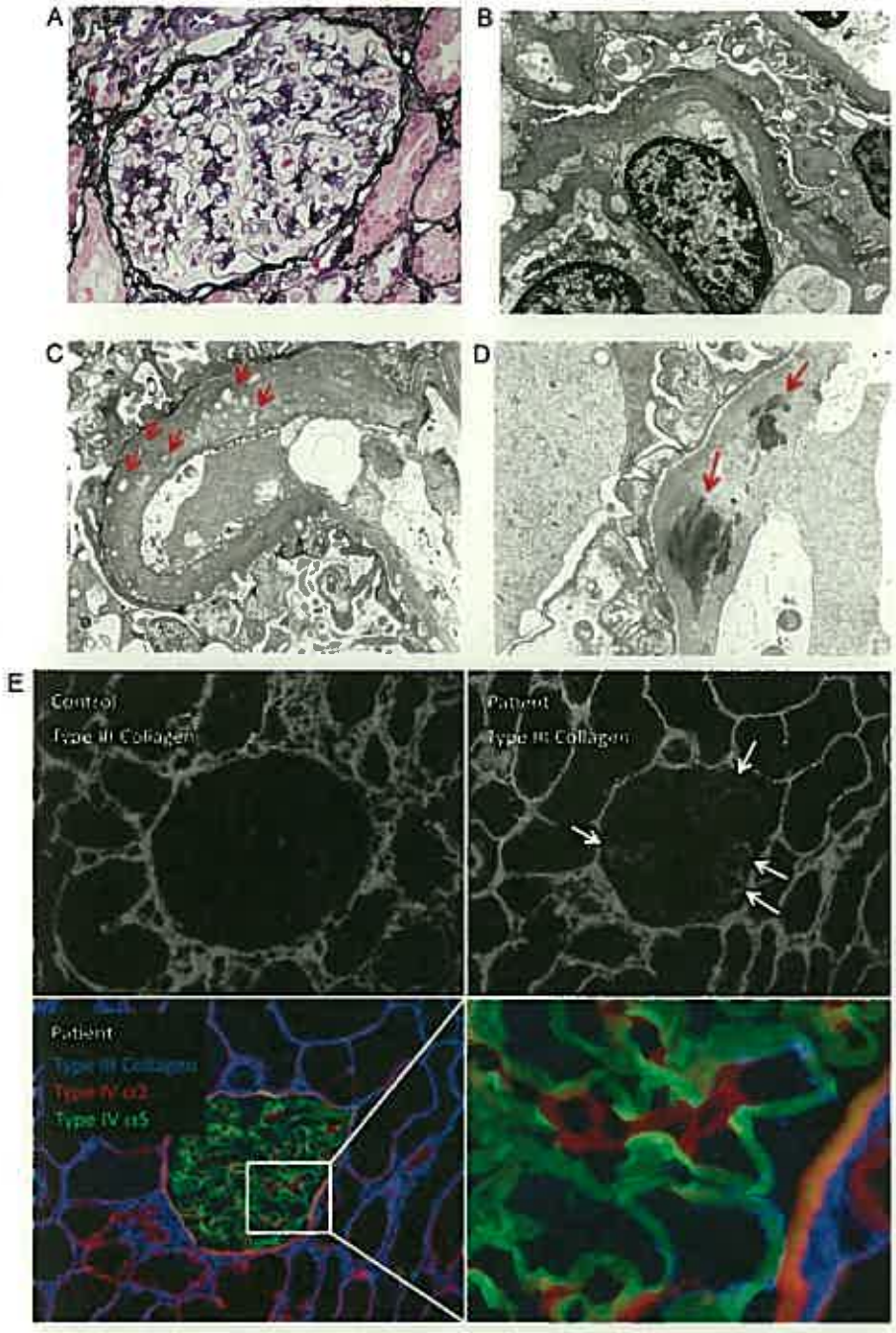

FIGURE 1: Renal histology of the NPLRD patient. (A) Light microscopy shows a normal glomerulus (Periodic acid-methenamine-silver stain, original magnification: ×400). Capillaries are patent and the GBM appears to be normal in thickness, contour and texture. The interstitium, renal tubules and vessels are normal. (B and C) Electron microscopic analysis. Partial effacement of the podocyte foot processes was observed, and the GBM was irregularly thickened (B, magnification: ×3000). The GBM had a moth-eaten appearance (red arrows), which is often seen in patients with NPS nephropathy (C, magnification: ×10 000). (D) Tannic acid staining (magnification: ×20 000) shows fibrillar material embedded in the GBM (red arrows). (E) Immunohistological analysis. Blue, red and green signals indicated Type III collagen, α2 chain of Type IV collagen and α5 chain of Type IV collagen, respectively. Type III collagen is not expressed in control glomeruli (upper left); however, its expression was increased in the glomeruli (upper right). It is expressed in the GBM and co-localized with Type IV collagen (lower panels). No decrease in the expression level of the α2 and α5 chains of Type IV collagen was observed.

fetal bovine serum in humidified 95% air and 5% CO_2 at 37°C. Cells cultured in 24-well plates were transfected with 900 ng DNA, including 100 ng of the reporter gene, 10 ng shPAN1-pBAT14, the indicated amount of each LMX1B expression plasmids and 5 ng pRL-CMV (Promega, Madison, WI, USA) using Lipofectamine 2000 (Invitrogen). After 24 h, the

transcriptional activity was assayed using a Dual-Luciferase Reporter Assay System (Promega). The luciferase activities of 5xFar/FLAT-pFOXluc1.prl were normalized to those of pRL-CMV.

RESULTS

Patient clinical observation

The patient was a 6-year-old Japanese girl with mild proteinuria and microscopic haematuria detected by chance. No familial history of renal disease or nail or skeletal abnormalities were detected. Physical examination and patellar radiography confirmed normal nails, normal patella, no iliac horns, no elbow dysplasia, no hairline abnormalities, no low proximal muscle mass of the limbs, no swan-neck deformity of the fingers, no Lester's sign in the iris and normal intraocular pressure. Blood biochemical examinations were within normal limits (blood urea nitrogen, 13.3 mg/dL; creatinine, 0.26 mg/dL; cystatin C, 0.62 mg/dL and IgA, 171 mg/dL). Urinalysis revealed proteinuria at a level of 1 g/g creatinine, and urine sediments showed 10–19 red blood cells per high power field. Renal biopsy was performed for further investigation of persistent proteinuria. The same levels of proteinuria and haematuria persisted for the 3 years subsequent to renal biopsy.

Morphological findings

Light microscopy revealed normal glomeruli (Figure 1A) and no abnormality of the GBM. No specific deposition of immunoglobulin G, A or M, nor of complements C3 and C4, was detected by direct immunofluorescence (Supplementary Figure S1). Electron microscopy revealed moderate effacement of podocyte foot processes (Figure 1B). The GBM was irregularly thickened (Figure 1B), and had a moth-eaten appearance (Figure 1C), which is often observed in patients with NPS nephropathy. Fibrillar materials embedded in the GBM were demonstrated in tannic acid-stained sections (Figure 1D), and an immunofluorescent analysis demonstrated that these fibrillar materials consisted of Type III collagen (Figure 1E). Based on the typical electron microscopic appearance together with the absence of nail and skeletal dysplasia, a diagnosis of NPLRD was made.

Next, immunohistological analysis was performed to elucidate the alteration of podocytes. No difference in the expression of slit diaphragm proteins (nephrin, podocin and ZO-1), cytoskeletal proteins (synaptopodin, vimentin, ezrin and GLEPP-1) and WT1 was detected from those in control subjects (Figure 2). On the other hand, the expression of CD2AP, which was evenly stained in control podocytes, was altered to a cytoplasmic granular pattern in our patient (Figure 3). This change was not accompanied by podocin or synaptopodin alterations, both of which interact with CD2AP [19, 20].

Analysis of *LMX1B* mutation

A sequence analysis of *LMX1B* revealed a heterozygous G-to-A transition in exon 4. This mutation is predicted to result in the substitution of arginine to glutamine in codon 246 (R246Q) (Figure 4A). R246Q is a novel mutation, although

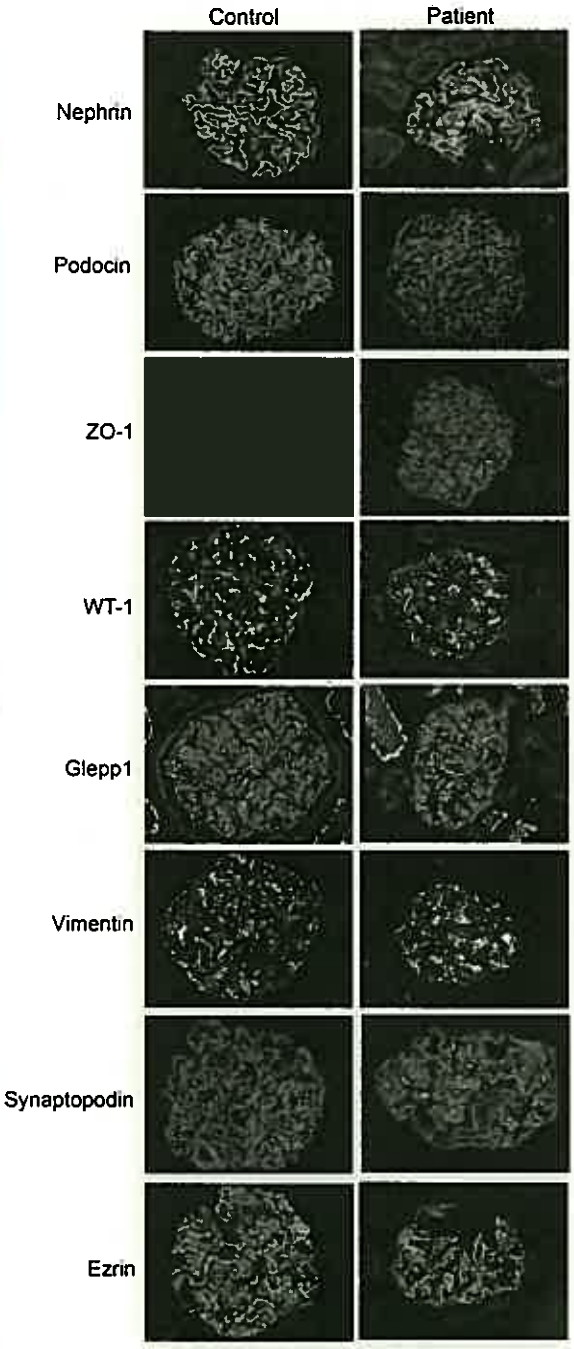

FIGURE 2: Immunohistological analysis of podocyte protein expression in glomeruli from normal controls and the patient. No difference in the expression levels of nephrin, podocin, ZO-1. WT1, GLEPP1, vimentin or ezrin was observed (magnification: ×400).

nonsense mutations (R246X) resulting in typical NPS have been reported in the same residue [7]. R246Q is not registered in the database of single-nucleotide polymorphisms (SNPs) of the National Center for Biotechnology Information (dbSNP, www.ncbi.nlm.nih.gov) nor in the Japanese SNP control database established by the National Bioscience Data Base Center, which has genome-wide data for a million SNPs from 700

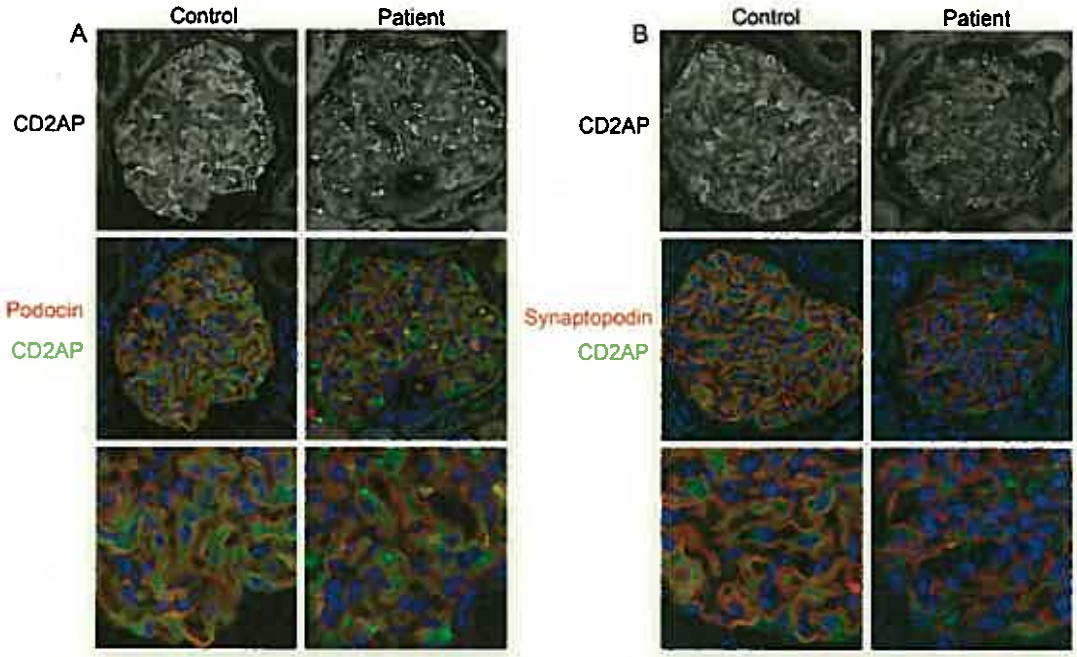

FIGURE 3: Immunohistological analysis of CD2AP in glomeruli from normal controls and the patient. Upper panels: CD2AP, middle panels: co-staining with podocin (A) or synaptopodin (B), bottom panels: enlarged view of middle panels. In the NPLRD patient, CD2AP expression pattern was altered from linear to granular. Note that granular CD2AP signals did not co-localize with podocin (A) or synaptopodin (B) (magnification: ×400).

samples (http://gwas.biosciencedbc.jp/snpdb/snp_top.php). In this study, the absence of this DNA sequence abnormality in 100 alleles from 50 unrelated healthy Japanese individuals indicated that R246Q is a mutation and not a polymorphism. R246 is located in the homeodomain and is well conserved among human LMX1B, mouse Lmx1b, Xenopus Lmx1b, human LMX1A [17] and human homeobox protein engrailed. As amino acid residue comprises the DNA-binding motif, which inserts into the minor groove of DNA, R246Q may have a critical influence on LMX1B function. We also assessed the functionality of R246Q using the Sorting Intolerant From Tolerant (SIFT) web-based tool (http://sift.jcvi.org) and the Polymorphism Phenotyping 2 (PolyPhen2) tool (http://genetics.bwh.harvard.edu/pph2) by homology modelling and threading, which predicted R246Q as 'damaging' and 'probably damaging', respectively.

Transcriptional activity of LMX1B mutants

To examine the effect of R246Q on LMX1B transactivation, LMX1B-wild type and LMX1B-R246Q were transiently overexpressed in Cos-1 cells, and the transcriptional activity was analysed by luciferase reporter assay. The same experiments were also performed with another mutation (V265L reported as V242L), which was identified in a patient with typical NPS, and negligible transcriptional activity was found [15]. A mini-enhancer of the rat insulin I gene was used, the E2A3/4 (Far/FLAT) sequence, which is bound to and transactivated by LMX1B [17].

Transcriptional activity of the LMX1B-wild type increased in a dose-dependent manner, and that of LMX1B-V265L was negligible, as previously reported [15]. On the other hand, transcriptional activity of LMX1B-R246Q was significantly lower than that of LMX1B-wild type at low doses, but showed comparable activity at a high dose (Figure 4B). The transcriptional activity of LMX1B-R246Q at the higher dose was significantly greater than that of LMX1B-V265L. These results revealed that transcriptional activity of LMX1B-R246Q was only partially impaired.

Because R246Q was detected heterozygously, the possibility of a dominant-negative effect of LMX1B-R246Q on the LMX1B-wild type was examined. The LMX1B-wild type was transfected with increasing amounts of LMX1B-R246Q in Cos-1 cells. The results indicated that LMX1B-R246Q manifested no dominant-negative effect, but rather had an additional positive effect on the transcriptional activity of LMX1B-wild type (Figure 4C, lanes 1–5). When an equal amount of LMX1B-R246Q was transfected with LMX1B-wild type, the transcriptional activities of mixed LMX1B-R246Q and LMX1B-wild type were significantly lower than that of LMX1B-wild type alone (Figure 4C, lanes 6 and 7). These results indicated that, in the heterozygous state, the R246Q mutant has no dominant-negative effect, but reduces transcriptional activity more than the wild type in its homozygous state.

DISCUSSION

This is the first report identifying heterozygous *LMX1B* mutation in a patient with NPLRD in whom isolated glomerulopathy with characteristic histology of NPS nephropathy was observed. As R246 is located in the homeodomain and is well conserved in different species, R246Q mutation may have a critical influence on *LMX1B* function. The functioning of the detected mutation assessed by SIFT and PolyPhen2 supported

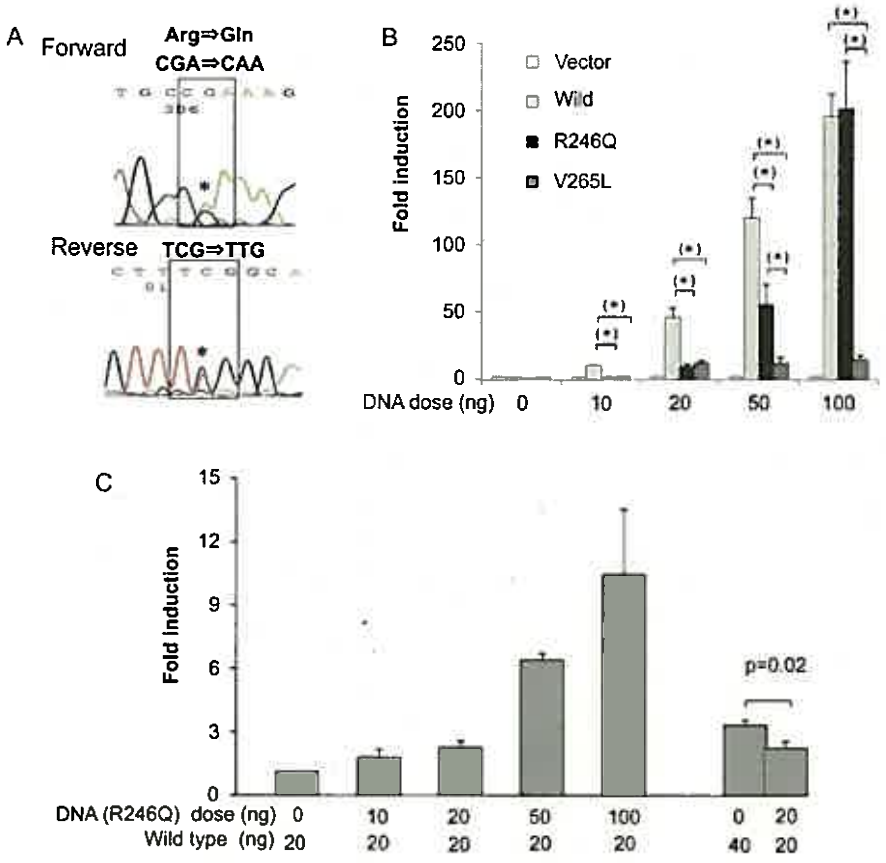

FIGURE 4: (A) R246Q was identified in a patient with NPLRD. A heterozygous G-to-A transition was detected in exon 4, which is predicted to result in substitution of Arg to Gln in codon 246 (R246Q). (B) The transcriptional activity of LMX1B-R246Q. The indicated amounts of each LMX1B expression plasmid were transfected with 100 ng of the insulin mini-enhancer reporter into Cos-1 cells. The relative luciferase activity (Firefly/Renilla) was measured in three independent experiments. Fold induction refers to the activity with no LMX1B. Error bars represent standard deviation. Asterisks indicate statistical differences at $P < 0.001$. (C) Analysis of the dominant-negative effect of LMX1B-R246Q on LMX1B-wild type transcriptional activity. The indicated amounts of LMX1B-R246Q were co-transfected with LMX1B-wild type and 100 ng of the insulin mini-enhancer reporter into Cos-1 cells. The relative luciferase activity (Firefly/Renilla) was measured in three independent experiments. Fold induction refers to the activity with 20 ng of the LMX1B-wild type. Error bars represent standard deviation.

this prediction. In fact, significantly lower transcriptional activity was observed with LMX1B-R246Q than that with the LMX1B-wild type at low doses, although LMX1B-R246Q transcriptional activity was similar to that of the LMX1B-wild type at higher doses. Moreover, heterozygosity in R246Q/wild type was associated with lower transcriptional activity than the wild type (Figure 4C). No mutation was found in the apparently normal parents, which matches the co-segregation of the mutation with the phenotype. Taken together, we consider that R246Q in the *LMX1B* was the causative mutation for the NPLRD phenotype in our patient.

It is widely accepted that a reduced dosage of the LMX1B protein causes NPS, and that loss of function is the predominant mechanism underlying NPS pathogenesis [15, 17, 21]. In a murine model, *Lmx1b*-null mice immediately died after birth due to massive glomerular vascular leaks, while heterozygous *Lmx1b*$^{+/-}$ mice did not manifest this renal phenotype. On the other hand, human NPS is caused by LMX1B haploinsufficiency. In this study, NPLRD was also caused by LMX1B haploinsufficiency. In our patient, heterozygous *LMX1B* mutation caused no nail or skeletal abnormalities, although these are seen in 98 and >90% NPS patients, respectively [3]. In this study, partially defective transcriptional activity of R246Q was identified. R246Q function was adequate for ungual and patellar development, but insufficient for normal glomerular formation or maintenance. Although NPLRD pathogenesis cannot be determined from the evidence of only one case, the findings here indicate that differences between NPS and NPLRD may be explained by the partially defective transcriptional activity of R246Q in patients with NPLRD.

How do defects in LMX1B transcription activity affect the renal phenotype? Lmx1b is exclusively expressed in the glomeruli of mouse kidney [9], and podocyte foot processes are defective in *Lmx1b*-null mice [22]. Furthermore, podocyte-specific knockout of *Lmx1b* in mice causes foot process effacement [9]. These results indicate that thickening of the GBM, effacement of foot processes as well as proteinuria and haematuria in NPS nephropathy are caused by podocyte defects. Downstream targets of LMX1B in podocytes remain largely unknown. *Lmx1b*-null mice exhibit abnormal GBM

ultrastructures and strong reduction in glomerular expression of the Type IV collagen α3 and α4 chains, podocin and CD2AP [22]. However, in typical NPS patients with a thickened GBM and deposition of collagen Type III in the GBM, podocyte protein expression is well conserved [10]. In our patient with NPLRD who presented with mild but distinct proteinuria, foot process effacement and collagen Type III deposition, the levels of expression of slit diaphragm proteins (nephrin, podocin and ZO-1) and cytoskeletal proteins (synaptopodin and vimentin) in podocytes were maintained (Figure 2). On the other hand, CD2AP expression patterns were altered from linear to granular in our NPLRD patient (Figure 3). CD2AP is a multifunctional adaptor molecule localized to the cytoplasm and slit diaphragm in podocytes. It plays a role in cytoskeletal remodelling, cell survival and endocytosis [19, 20, 23]. The COOH terminus of CD2AP interacts directly with filamentous actin, synaptopodin, nephrin and podocin and serves as a link anchoring slit membrane proteins to the actin cytoskeleton of podocytes [19, 20, 23]. In our patient, granular signals for CD2AP did not co-localize with those for synaptopodin or podocin, suggesting that LMX1B may affect its expression or interaction with these proteins. It is also possible that LMX1B regulates transcription of unknown molecules critical to the proper cytoplasmic localization of CD2AP. From these results, in addition to regulation of collagen Type III expression by LMX1B directly or indirectly, it is presumed that LMX1B may regulate transcriptional activity by targeting the formation or maintenance of podocyte structure.

Our results suggest the possibility that even some minor urinary abnormalities are caused by *LMX1B* mutation, although only a few cases are reported as NPLRD in the literature [7, 11, 12]. In our patient, mild proteinuria and haematuria were detected by chance, and no progression was observed during a follow-up period of 3 years. Diagnosis of NPLRD is only possible by electron microscopy. It is characterized by intramembranous fibrillar collagen accumulation in the GBM. However, it may sometimes be only poorly visualized using routine electron microscopic staining techniques and may require double staining for adequate NPLRD demonstration [12]. Our results shed light on the role of *LMX1B* in the pathogenesis of isolated glomerular diseases, which, together with nephropathy in NPS, can be designated as 'LMX1B nephropathy'.

In conclusion, we identified a novel *LMX1B* mutation (R246Q) resulting in reduced transcriptional activity in a patient with NPLRD. NPLRD may be caused by *LMX1B* mutations and residual transcriptional activity, which results in deformation of the GBM and podocytes. However, the possibility cannot be ruled out that mutations or variants in other genes may be responsible for or have an additive effect on this phenotype. Collagen Type III staining in the GBM and/or *LMX1B* analysis is needed in patients with isolated glomerulopathy especially those with GBM irregularity by the routine electron microscopic study, and in those with a family history of the NPS phenotype or dominant inheritance. Analyses of additional cases are vital to elucidate the role of *LMX1B* in isolated glomerular diseases.

ACKNOWLEDGEMENT

We thank Dr Brendan Lee and Dr Michael S. German for providing the plasmids, and Minako Takaki and Yukiko Matsuo for technical supports, and Mitsuko Itoh for kind assistance in English usage. This study was supported by grant-in-aid from the Ministry of Education, Science, Sports and Culture of Japan.

SUPPLEMENTARY DATA

Supplementary data are available online at http://ndt.oxfordjournals.org.

CONFLICT OF INTEREST STATEMENT

None declared.

REFERENCES

1. Beals RK, Eckhardt AL. Hereditary onycho-osteodysplasia (nail-patella syndrome). A report of nine kindreds. J Bone Joint Surg Am 1969; 51: 505–516
2. Lichter PR, Richards JE, Downs CA *et al.* Cosegregation of open-angle glaucoma and the nail-patella syndrome. Am J Ophthalmol 1997; 124: 506–515
3. Sweeney E, Fryer A, Mountford R *et al.* Nail patella syndrome: a review of the phenotype aided by developmental biology. J Med Genet 2003; 40: 153–162
4. Vollrath D, Jaramillo-Babb VL, Clough MV *et al.* Loss-of-function mutations in the LIM-homeodomain gene, LMX1B, in nail-patella syndrome. Hum Mol Genet 1998; 7: 1091–1098
5. Dreyer SD, Zhou G, Baldini A *et al.* Mutations in LMX1B cause abnormal skeletal patterning and renal dysplasia in nail patella syndrome. Nat Genet 1998; 19: 47–50
6. Chen H, Lun Y, Ovchinnikov D *et al.* Limb and kidney defects in Lmx1b mutant mice suggest an involvement of LMX1B in human nail patella syndrome. Nat Genet 1998; 19: 51–55
7. Bongers EM, Gubler MC, Knoers NV. Nail-patella syndrome. Overview on clinical and molecular findings. Pediatr Nephrol 2002; 17: 703–712
8. Lemley KV. Kidney disease in nail-patella syndrome. Pediatr Nephrol 2009; 24: 2345–2354
9. Suleiman H, Heudobler D, Raschta AS *et al.* The podocyte-specific inactivation of Lmx1b, Ldb1 and E2a yields new insight into a transcriptional network in podocytes. Dev Biol 2007; 304: 701–712
10. Heidet L, Bongers EM, Sich M *et al. In vivo* expression of putative LMX1B targets in nail-patella syndrome kidneys. Am J Pathol 2003; 163: 145–155
11. Salcedo JR. An autosomal recessive disorder with glomerular basement membrane abnormalities similar to those seen in the nail patella syndrome: report of a kindred. Am J Med Genet 1984; 19: 579–584

12. Zuppan CW, Weeks DA, Cutler D. Nail-patella glomerulopathy without associated constitutional abnormalities. Ultrastruct Pathol 2003; 27: 357–361
13. Harita Y, Kurihara H, Kosako H *et al.* Phosphorylation of nephrin triggers Ca2+ signaling by recruitment and activation of phospholipase C-gamma 1. J Biol Chem 2009; 284: 8951–8962
14. Kajiho Y, Harita Y, Kurihara H *et al.* SIRPalpha interacts with nephrin at the podocyte slit diaphragm. FEBS J 2012; 279: 3010–3021
15. Sato U, Kitanaka S, Sekine T *et al.* Functional characterization of LMX1B mutations associated with nail-patella syndrome. Pediatr Res 2005; 57: 783–788
16. German MS, Wang J, Chadwick RB *et al.* Synergistic activation of the insulin gene by a LIM-homeodomain protein and a basic helix-loop-helix protein: building a functional insulin minienhancer complex. Genes Dev 1992; 6: 2165–2176
17. Dreyer SD, Morello R, German MS *et al.* LMX1B transactivation and expression in nail-patella syndrome. Hum Mol Genet 2000; 9: 1067–1074
18. German M, Ashcroft S, Docherty K *et al.* The insulin gene promoter. A simplified nomenclature. Diabetes 1995; 44: 1002–1004
19. Huber TB, Kwoh C, Wu H *et al.* Bigenic mouse models of focal segmental glomerulosclerosis involving pairwise interaction of CD2AP, Fyn, and synaptopodin. J Clin Invest 2006; 116: 1337–1345
20. Schwarz K, Simons M, Reiser J *et al.* Podocin, a raft-associated component of the glomerular slit diaphragm, interacts with CD2AP and nephrin. J Clin Invest 2001; 108: 1621–1629
21. Bongers EM, de Wijs IJ, Marcelis C *et al.* Identification of entire LMX1B gene deletions in nail patella syndrome: evidence for haploinsufficiency as the main pathogenic mechanism underlying dominant inheritance in man. Eur J Hum Genet 2008; 16: 1240–1244
22. Miner JH, Morello R, Andrews KL *et al.* Transcriptional induction of slit diaphragm genes by Lmx1b is required in podocyte differentiation. J Clin Invest 2002; 109: 1065–1072
23. Huber TB, Hartleben B, Kim J *et al.* Nephrin and CD2AP associate with phosphoinositide 3-OH kinase and stimulate AKT-dependent signaling. Mol Cell Biol 2003; 23: 4917–4928

Received for publication: 2.5.2013; Accepted in revised form: 15.7.2013

Bone Reports 2 (2015) 68–73

Contents lists available at ScienceDirect

Bone Reports

journal homepage: www.elsevier.com/locate/bonr

Case Report

Hereditary 1,25-dihydroxyvitamin D-resistant rickets (HVDRR) caused by a *VDR* mutation: A novel mechanism of dominant inheritance

Tsuyoshi Isojima [a], Michiyasu Ishizawa [b], Kazuko Yoshimura [c], Mayuko Tamura [a], Shinichi Hirose [c], Makoto Makishima [b], Sachiko Kitanaka [a,*]

[a] Department of Pediatrics, Graduate School of Medicine, The University of Tokyo, 7-3-1 Hongo, Bunkyo-ku, Tokyo 113-8655, Japan
[b] Division of Biochemistry, Department of Biochemical Sciences, Nihon University School of Medicine, 30-1 Oyaguchi-kamicho, Itabashi-ku, Tokyo 173-8610, Japan
[c] Department of Pediatrics, School of Medicine, Fukuoka University, 7-45-1 Nanakuma, Jonan-ku, Fukuoka 814-0180, Japan

ARTICLE INFO

Article history:
Received 16 April 2015
Accepted 6 May 2015
Available online 7 May 2015

Keywords:
Hereditary vitamin D resistant rickets
Dominant negative effect
Vitamin D receptor

ABSTRACT

Hereditary 1,25-dihydroxyvitamin D-resistant rickets (HVDRR) is caused by mutations in the *VDR* gene, and its inheritance is autosomal recessive. In this report, we aimed to confirm whether HVDRR is occasionally inherited as a dominant trait. An 18-month-old Japanese boy was evaluated for short stature and bowlegs. His father had been treated for rickets during childhood, and his paternal grandfather had bowlegs. We diagnosed him with HVDRR based on laboratory data and radiographic evidence of rickets. Sequence analyses of *VDR* were performed, and the functional consequences of the detected mutations were analyzed for transcriptional activity, ligand binding, and interaction with the retinoid X receptor, cofactors, and the vitamin D response element (VDRE). A novel mutation (Q400LfsX7) and a reported variant (R370H) were identified in the patient. Heterozygous Q400LfsX7 was detected in his father, and heterozygous R370H was detected in his healthy mother. Functional studies revealed that the transcriptional activity of Q400LfsX7-VDR was markedly disturbed. The mutant had a dominant-negative effect on wild-type-VDR, and the ligand binding affinity of Q400LfsX7-VDR was completely impaired. Interestingly, Q400LfsX7-VDR had a strong interaction with corepressor NCoR and could interact with VDRE without the ligand. R370H-VDR was functionally similar to wild-type-VDR. In conclusion, we found a dominant-negative mutant of VDR causing dominantly inherited HVDRR through a constitutive corepressor interaction, a mechanism similar to that in dominantly inherited thyroid hormone receptor mutations. Our report together with a reported pedigree suggested a distinct inheritance of HVDRR and enriched our understanding of VDR abnormalities.

1. Introduction

The hormonal metabolite of vitamin D, 1,25-dihydroxyvitamin D [1,25$(OH)_2D_3$] regulates calcium homeostasis, cellular differentiation, and immune function through its binding to the vitamin D receptor (VDR), a transcription factor belonging to the steroid/nuclear receptor superfamily (Feldman and Malloy, 2014; Haussler et al., 2013; Rachez and Freedman, 2000; Malloy et al., 2011). The regulation of specific gene transcription by VDR requires it to form a heterodimer with the retinoid X receptor (RXR); this heterodimer then binds to vitamin D response elements (VDREs) in the promoter region of target genes, releasing corepressor proteins and recruiting coactivator proteins. 1,25$(OH)_2D_3$ binding to VDR causes the repositioning of helix H12, which contains an activation function 2 (AF-2) domain, allowing for the recruitment of coactivators (Rochel et al., 2000).

Hereditary 1,25-dihydroxyvitamin D-resistant rickets (HVDRR) (OMIM #277440), also known as vitamin D-resistant rickets type 2A, is a rare monogenic disorder caused by mutations in the *VDR* gene (Malloy and Feldman, 2010). Patients with HVDRR often have consanguinity in the family and display a number of clinical features including early onset rickets, hypocalcemia, and secondary hyperparathyroidism. Moreover, they have significantly elevated serum 1,25$(OH)_2D$ levels; this differentiates this condition from 1α-hydroxylase deficiency, also known as vitamin D-dependent rickets type 1A (Kitanaka et al., 1998). Multiple mutations in the *VDR* gene have been reported to cause HVDRR (Malloy et al., 2014). Mutations in the DNA binding domain (DBD) of the *VDR* gene interfere with VDR–DNA interactions and result in the loss of VDR function, and these are usually associated with alopecia (Malloy et al., 2014). Mutations in the *VDR* ligand binding domain (LBD) alter the ligand binding affinity in various ways. These LBD mutations can result in partial or total hormone unresponsiveness and can be associated with alopecia (Malloy et al., 2002).

Patients with HVDRR usually have biallelic mutations in the *VDR* gene (Feldman and Malloy, 2014). Those with heterozygous mutations

* Corresponding author.
E-mail address: sachi-tky@umin.ac.jp (S. Kitanaka).

http://dx.doi.org/10.1016/j.bonr.2015.05.001

(i.e., the parents of sufferers) show no symptoms and have normal bone development (Malloy et al., 2004, 2011). Recently, a single family has been reported to demonstrate dominant inheritance caused by a *VDR* mutation with a dominant-negative effect (Malloy et al., 2011). Here, we report a family with HVDRR showing dominant inheritance, in which we identified a novel mutation with a dominant-negative effect and enhanced corepressor interaction. This is the first report of a dominant-negative VDR mutation demonstrating a constitutive corepressor interaction, a mechanism similar to that in dominantly inherited thyroid hormone receptor (TR) mutations (Safer et al., 1998; Liu et al., 1998; Fozzatti et al., 2011, 2013; Bochukova et al., 2012).

2. Subjects and methods

2.1. Patient clinical observation

An 18-month-old Japanese boy was referred to our institute and evaluated for short stature and bowlegs. His body length and weight were 80.2 cm [−2.0 standard deviations (SD)] and 8.6 kg (−1.6 SD), respectively. He is the first child of nonconsanguineous parents, and his birth history was unremarkable. He started walking at the age of 14 months, but his parents felt he had a slight waddling gait. Intellectual development was within normal limits. His father had been treated for a short period with some vitamin D for rickets during childhood, which was considered to be due to simple vitamin D deficiency; his height was 173 cm, and he had a slight bowing of his legs. The patient's paternal grandfather also had bowlegs without alopecia, although he had never been treated.

Radiographic study of the hands and knees was consistent with rickets (Fig. 1A). Blood biochemistry showed normal serum calcium (Ca) (2.2 mmol/l; reference range, 2.1–2.4) and 25(OH)D levels (20 ng/ml; insufficiency, <20). However, they showed slightly decreased serum phosphorus (P) (1.1 mmol/l; reference range, 1.3–2.0) and elevated serum alkaline phosphatase (ALP) (3346 U/l; reference range, 171–785), intact parathyroid hormone (iPTH) (480 pg/ml; reference range, 10–65), and $1,25(OH)_2D$ levels (304 pg/ml; reference range, 20–70). On the basis of these findings of obvious rickets, with elevated $1,25(OH)_2D$, ALP, and iPTH levels and a normal 25(OH)D level, we diagnosed him with HVDRR. However, we could not exclude the possibility of vitamin D deficiency. He was effectively treated with 2 μg alfacalcidol daily without any calcium supplements, and his rickets, ALP, iPTH levels improved. The dose was tapered and stopped at the age of 4 years. At the last follow-up (age,

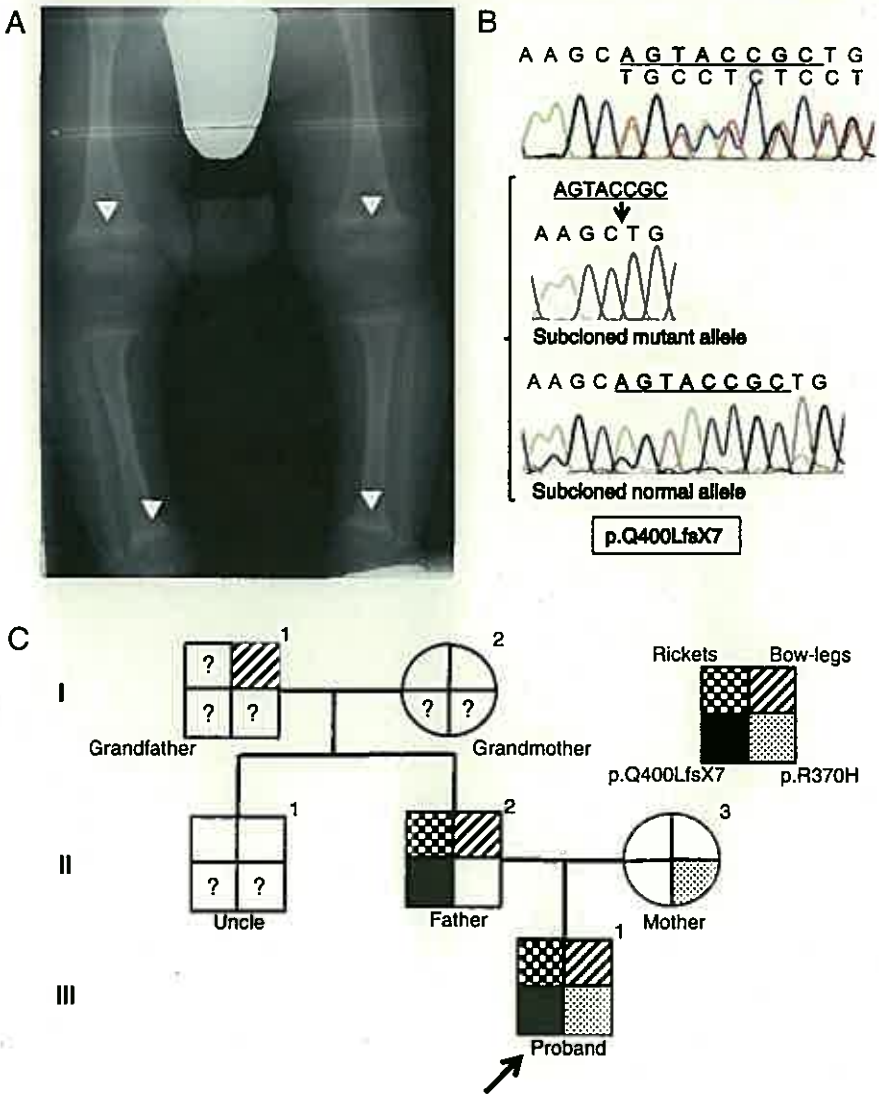

Fig. 1. Radiograph of the patient, a chromatogram of the novel mutation, and the family tree. (A) Radiograph of the patient at diagnosis. It showed cupping, fraying and flaring indicating that the patient had evident rickets. (B) The novel p.Q400LfsX7 mutation. In the chromatogram: nucleotides in bold black letters with underline indicate an 8-base pair deletion; and the lower part shows the subcloned normal and mutant sequences. (C) The pedigree analysis in this study.

5 years and 11 months), he had neither rickets nor alopecia and measured 106.8 cm (−1.3 SD) in height. His blood biochemistry showed normal Ca (2.4 mmol/l), P (1.5 mmol/l), ALP (622 U/l), and iPTH (53 pg/ml), but elevated $1,25(OH)_2D$ (271 pg/ml) levels.

2.2. VDR gene analysis

We obtained informed consent for DNA analysis from the parents, and the Ethics Committee of The University of Tokyo approved the study. Genomic DNA was extracted from peripheral white blood cells using a QIAamp DNA Blood Midi Kit (Qiagen, Hilden, Germany). The entire coding region and exon–intron boundaries of the *VDR* gene were amplified from genomic DNA by polymerase chain reaction (PCR) using the designed PCR primers. The details of the primers and the PCR conditions will be provided on request. Subsequently, PCR products were sequenced using an ABI Prism BigDye Terminator Cycle Sequencing Ready Reaction Kit (PE Applied Biosystems, Foster City, CA) and the forward and reverse primers from the PCR amplification. Direct sequencing in both directions was performed on an autosequencer (ABI PRISM 310, Genetic Analyzer; Applied Biosystems). Detected mutations were confirmed by cloning the PCR products into the pCR 2.1 vector using a TOPO TA Cloning kit (Invitrogen, Carlsbad, CA, U.S.A.). The clones derived from both alleles were sequenced.

2.3. Construction of plasmids

Expression plasmids for wild-type full-length human VDR or RXRα and a reporter plasmid for human 24-hydroxylase promoter (−367 to 0) in pGL3 were provided by S. Kato. The expression plasmids hVDR-pCMX, hVDR-flag-pCMX, hVDR-VP16-pCMX, RXRα-GAL4-pCMX, GRIP1-GAL4-pCMX, and NCoR-GAL4-pCMX have been reported previously (Inaba et al., 2007). GAL4-responsive MH100(UAS)x4-tk-LUC and VDR-responsive Sppx3-tk-LUC were also used in the luciferase reporter assay (Nakano et al., 2005; Igarashi et al., 2007). The mutant plasmids (Q400LfsX7 and R370H) were created with a Quick Change Site-directed mutagenesis kit (Stratagene, La Jolla, CA) according to the manufacturer's protocol (Sato et al., 2005). *VDR* mutant constructs were sequence-verified to have no extra mutations.

2.4. Transcriptional activity

COS-1 cells were cultured in Dulbecco's modified Eagle's medium (DMEM) supplemented with 10% fetal bovine serum, 100 unit/ml penicillin, and 100 μg/ml streptomycin at 37 °C in a humidified atmosphere containing 5% CO_2. Transfections in COS-1 cells were performed by modification of previously reported methods (Sato et al., 2005; Jurutka et al., 2000). Cells that were cultured in 24-well plates were transfected with 800 ng DNA, including 300 ng 24-hydroxylase-pGL3 promoter luciferase, the indicated amounts of each human VDR expression plasmids, and 1 ng pRL-CMV (Promega, Madison, WI) using Lipofectamine 2000 (Invitrogen, Carlsbad, CA). Four hours after transfection, the indicated amounts of ligand were added. After 24 h, transcriptional activity was assayed using a Dual-Luciferase Reporter Assay System (Promega). The luciferase activities of human 24-hydroxylase promoter luciferase plasmid were normalized to the luciferase activities of pRL-CMV. Transient transfections were performed in triplicate, and each experiment was repeated at least three times.

2.5. Mammalian two-hybrid analyses

Human embryonic kidney (HEK) 293 cells were cultured in DMEM containing 5% fetal bovine serum and an antibiotic–antimycotic (Nacalai, Kyoto) at 37 °C in a humidified atmosphere containing 5% CO_2. Transfections in HEK293 cells were performed by the calcium phosphate coprecipitation analysis as described previously (Adachi et al., 2005). Cells that were cultured in 96-well plates were transfected with 50 ng GAL4-responsive MH100(UAS)x4-tk-LUC reporter plasmid or VDR-responsive Sppx3-tk-LUC, 20 ng β-galactosidase-pCMX, 15 ng of each VDR, and/or the cofactor expression plasmid and pGEM carrier DNA for a total 150 ng DNA. Eight hours after transfection, the indicated amounts of ligands were added. Cells were harvested approximately 16–24 h after treatment, and luciferase and β-galactosidase activities were assayed using a luminometer and a microplate reader (Molecular Devices, Sunnyvale, CA). Luciferase data were normalized to an internal β-galactosidase control and were represented as the mean (±SD) of triplicate assays.

2.6. Competitive ligand-binding assay

LBDs of human *VDR* and its mutants were cloned into the GST-fusion vector pGEX-4T1 (Amersham Pharmacia Biotech, Piscataway, NJ). GST–VDR fusion proteins were expressed in BL21 DE3 cells (Promega) and purified with glutathione sepharose beads (Amersham Pharmacia Biotech). A competitive ligand-binding assay was performed by modification of previously reported methods (Nakajima et al., 1994; Solomon et al., 2001). Briefly, 500 ng GST fusion proteins were bound to glutathione sepharose and incubated with [26,27-methyl-^{3}H]$1\alpha,25(OH)_2D_3$ (Amersham Pharmacia Biotech) in the presence or absence of the non-radioactive ligand in a buffer (10 mM Tris–HCl, pH 7.6; 1 mM EDTA; 300 mM KCl; 1 mM dithiothreitol; 10% glycerol) for 3 h at 4 °C. After washing twice, the protein and bound $1\alpha,25(OH)_2D_3$ were resuspended in 200 μl of the binding buffer, and a 150 μl sample was assessed by liquid scintillation counting.

3. Results

3.1. Mutation analysis of the VDR gene

The genomic analyses for the *VDR* gene revealed that the patient had a novel deletion mutation and a reported variant (rs202139940). The mutation is an 8-base pair deletion in exon 10 of the *VDR* gene, c.1199–1206 del, p.Q400LfsX7, which is predicted to result in a frameshift from codon 400 and premature termination just before helix H12 (Fig. 1B). This detected mutation was heterozygous in his father. The variant (rs202139940) is a G>A transition in exon 10 of the *VDR* gene, which is predicted to result in a substitution of arginine to histidine in codon 370 (R370H). This variant was also found to be heterozygous in his healthy mother. Both the patient and his mother were heterozygous for the *FokI* polymorphism (F/f) that alters the translational site from M1 to M4 (Jurutka et al., 2000; Haussler et al., 1998), while his father was homozygous for the f/M1 alleles.

3.2. Transcriptional activity of Q400LfsX7-VDR and R370H-VDR

To examine whether the detected Q400LfsX7 mutation and the R370H variant can affect VDR transactivation, wild-type Q400LfsX7-VDR and R370H-VDR were transiently overexpressed in COS-1 cells, and transcriptional activity was analyzed using the reporter 24-hydroxylase promoter. R370H-VDR showed similar transcriptional activity to that of wild-type-VDR (Fig. 2A). However, Q400LfsX7-VDR had negligible transcriptional activity. Similar results were also observed in HEK293 cells (data not shown). These results indicated that the Q400LfsX7-VDR mutant had completely lost all transcriptional activities, whereas R370H remained normal.

3.3. The dominant-negative effect of Q400LfsX7-VDR on wild-type VDR

We hypothesize that the heterozygous Q400LfsX7 mutation was the molecular cause of his HVDRR. We examined the dominant-negative effect of Q400LfsX7-VDR on the wild-type product by increasing the mutant-to-wild-type protein ratio with 5 nM of $1,25(OH)_2D_3$. When equal amounts of wild-type VDR and Q400LfsX7-VDR proteins were

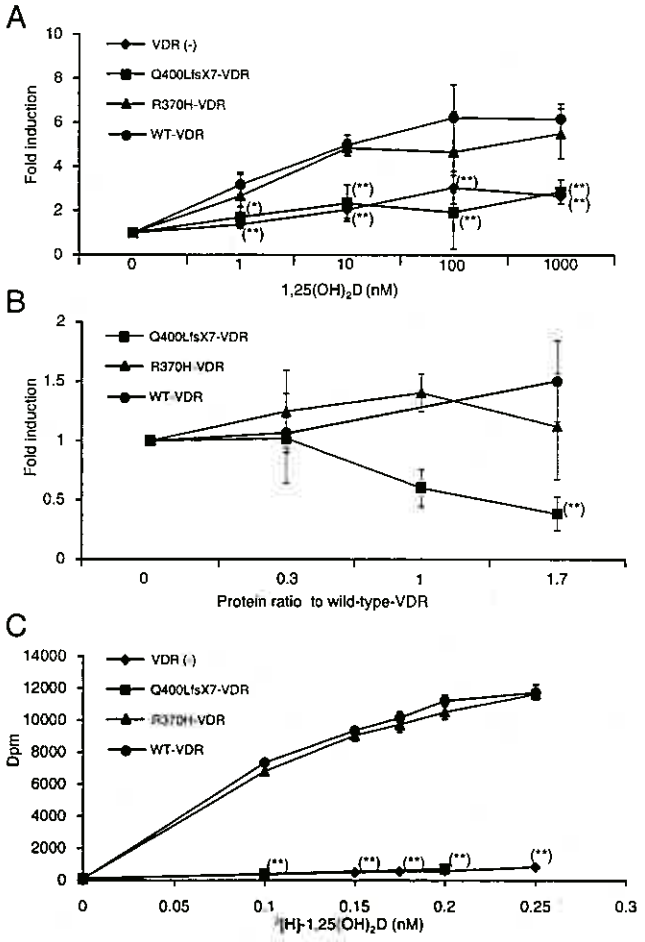

Fig. 2. Functional analysis of the VDR mutants. (Luciferase activity of the reporter is shown as relative light unit compared to that in cells transfected with control vector and treated with vehicle control. Error bars represent one standard deviation. (*) and (**) denote the statistically significant difference comparing to wild-type VDR at $p < 0.05$ and $p < 0.01$, respectively). (A) The transcriptional activity of Q400LfsX7 or R370H-VDR in COS-1 transfected cells. (B) Analysis of the dominant-negative effect of Q400LfsX7-VDR on wild-type-VDR transcriptional activity in COS-1 transfected cells with 5 nM of $1,25(OH)_2D_3$. (C) Direct binding of $1,25(OH)_2D_3$ to VDR. GST–VDR fusion proteins or GST control proteins incubated with increasing concentrations of $[^3H]1,25(OH)_2D_3$ in the presence or absence of 400-fold excess nonradioactive $1,25(OH)_2D_3$.

expressed, transcriptional activity was reduced by approximately 50%, and the increasing amounts of the mutant VDR further repressed wild-type VDR transcriptional activity (Fig. 2B). This finding demonstrated that Q400LfsX7-VDR had a dominant-negative effect on wild-type VDR. However, R370H-VDR did not affect wild-type VDR transcriptional activity (Fig. 2B). Moreover, Q400LfsX7-VDR showed a dominant-negative effect on R370H-VDR activity, similar to its effect on wild-type-VDR (data not shown). Similar results were observed in HEK293 cells using VDR-responsive Sppx3-tk-LUC (data not shown).

3.4. Ligand binding ability of Q400LfsX7-VDR and R370H-VDR

The binding affinity of $1,25(OH)_2D_3$ of Q400LfsX7 or R370H-VDR was examined by the competitive binding assay. Isotopically labeled $1,25(OH)_2D_3$ was incubated with glutathione-S-transferase (GST)-VDR proteins in the presence or absence of excess unlabeled $1,25(OH)_2D_3$, and specific binding of $1,25(OH)_2D_3$ was calculated. $[^3H]1,25(OH)_2D_3$ effectively bound to wild-type-VDR and R370H-VDR but did not bind to Q400LfsX7-VDR. This result indicated that ligand binding affinity of Q400LfsX7-VDR was completely impaired (Fig. 2C).

3.5. Interaction with RXR, coactivator, and corepressor of Q400LfsX7-VDR and R370H-VDR

Interactions between VDR mutants, RXR, the coactivator, or the corepressor were analyzed by a mammalian two-hybrid assay using hVDR-VP16-pCMX, RXRα-GAL4-pCMX, GRIP1-GAL4-pCMX, and NCoR-GAL4-pCMX, respectively. HEK293 cells were cotransfected with hVDR-VP16-pCMX, the MH100(UAS)x4-tk-LUC reporter, and RXRα-GAL4-pCMX and were treated with increasing concentrations of $1,25(OH)_2D_3$. R370H-VDR interacted with RXRα, similar to wild-type-VDR, in a dose-dependent manner of the ligand. However, Q400LfsX7-VDR did not interact with RXRα (Fig. 3A). This finding suggested that Q400LfsX-VDR had impaired heterodimerization with RXR. Next, we analyzed the interaction with a coactivator, GRIP1 (Fig. 3B). $1,25(OH)_2D_3$ induced concentration-dependent associations of GRIP1 with wild-type or R370H-VDR. On the other hand, the association of Q400LfsX7-VDR with GRIP1 was not identified in any amounts of $1,25(OH)_2D_3$ (Fig. 3B). Then, the interaction of VDR with a corepressor, NCoR, was evaluated with similar experiments (Fig. 3C). Wild-type or R370H-VDR showed an interaction with NCoR in the absence of the ligand, which decreased by adding $1,25(OH)_2D_3$. In contrast, Q400LfsX7-VDR had a strong interaction with NCoR, which did not decrease by adding $1,25(OH)_2D_3$ (Fig. 3C). These data indicated that Q400LfsX7 displayed a defective release of NCoR in response to the ligand.

3.6. VDRE interactions with Q400LfsX7-VDR or R370H-VDR

We next assessed the interaction of the VDR mutants and VDRE by transfecting VP16-VDR chimeric receptors together with the VDRE reporter. Because of ligand-independent activity, the luciferase activities of VP16 chimeric receptors showed an interaction between the receptor and the binding element (Makishima et al., 2002; Adachi et al., 2004; Endo-Umeda et al., 2012). HEK293 cells were transfected with VP16-VDR chimeric mutants together with the luciferase reporter containing a VDR-responsive everted repeat-6 element from the CYP3A4 promoter (Makishima et al., 2002). The activity was compared with the activity of those without VP16 to differentiate from transcriptional activity. Wild-type VP16-VDR or VP16-R370H-VDR induced luciferase activities in the absence of the ligand, and adding the ligand increased the activity (compare Fig. 3D lanes 5–12 with Fig. 3E lanes 5–12). This result suggested that these VDRs interacted with VDRE without the ligand and had ligand-dependent enhancement. In contrast, VP16-Q400LfsX7-VDR had ligand-independent activity (compare Fig. 3D lanes 13–16 with Fig. 3E lanes 13–16). Thus, Q400LfsX7-VDR could interact with VDRE, although the interaction was not influenced by the ligand (Fig. 3D lanes 13–16).

4. Discussion

We have identified and presented a novel *VDR* mutation (Q400LfsX7) with a dominant negative effect on wild-type-VDR in a family with dominantly inherited HVDRR. Because HVDRR is usually transmitted autosomal recessively, and because our patient had the R370H variant, we initially believed that the mutation and the variant were the molecular basis for his HVDRR. However, when we assessed the functionality of R370H [using the Sorting Intolerant from Tolerant (SIFT) web-based tool (http://sift.jcvi.org) and the Polymorphism Phenotyping 2 (PolyPhen2) tool (http://genetics.bwh.harvard.edu/pph2)] by homology modeling and threading, R370H was described as "tolerated" and "benign," respectively. Furthermore, considering that rickets was dominantly inherited in this family (Fig. 1C), and that the patient showed a clinical course similar to that shown by his father, who had

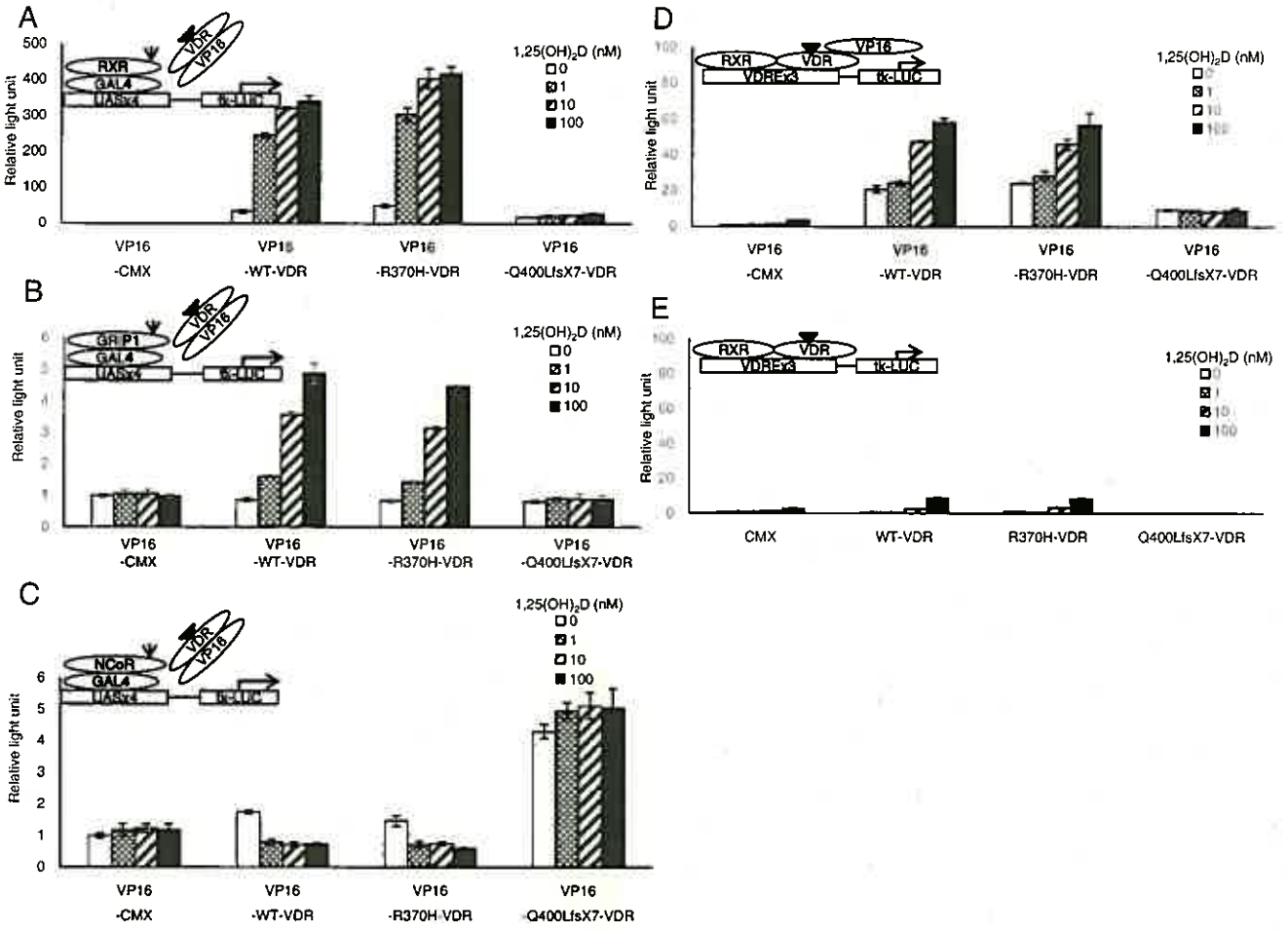

Fig. 3. RXR, coactivator, corepressor, and VDRE interactions with Q400LfsX7-VDR or R370H-VDR in HEK293 transfected cells. (Luciferase activity of the reporter is shown as relative light unit compared to that in cells transfected with control vector and treated with vehicle control. Error bars represent one standard deviation). (A) RXR interactions with Q400LfsX7-VDR or R370H-VDR. Mammalian two-hybrid analysis using hVDR-VP16-pCMX and RXRα-GAL4-pCMX in HEK293 cells. (B) Coactivator GRIP1 interactions with Q400LfsX7-VDR or R370H-VDR. Mammalian two-hybrid analysis using hVDR-VP16-pCMX and GRIP1-GAL4-pCMX in HEK293 cells. (C) Corepressor NCoR interactions with Q400LfsX7-VDR or R370H-VDR. Mammalian two-hybrid analysis using hVDR-VP16-pCMX and NCoR-GAL4-pCMX in HEK293 cells. (D) VDRE interactions with Q400LfsX7-VDR or R370H-VDR. VP16-VDR lanes. (E) VDRE interactions with Q400LfsX7-VDR or R370H-VDR. VDR lanes. Transcriptional activity of Q400LfsX7-VDR was augmented with a VP16 chimeric receptor in a ligand-independent manner (compare VP16-VDR lanes (panel D) to VDR lanes (panel E)).

an identical heterozygous Q400LfsX7 mutation, we hypothesized that this mutation was the more likely molecular cause of his HVDRR. Indeed, the function of R370H-VDR was almost identical to wild-type VDR, including its transcriptional activity, ligand binding, and interactions with RXR, cofactors, and VDRE (Figs. 2–3). Conversely, transcriptional activity and ligand binding ability of Q400LfsX7-VDR were completely impaired (Fig. 2A and C). More importantly, the mutant had a dominant-negative effect on wild-type-VDR (Fig. 2B). Thus, we concluded that the heterozygous Q400LfsX7 mutation caused the dominantly inherited HVDRR in this family through its dominant-negative effect on wild-type-VDR.

To our knowledge, this is the second reported pedigree of dominantly inherited HVDRR. The mutation detected in the first reported family (E420A) has been reported to show a dominant-negative effect (Malloy et al., 2011). In this study, we found that our Q400LfsX7 mutant differed from that in the previous report in terms of several functional properties. First, ligand binding was completely abolished in Q400LfsX7 (Fig. 2C), but remained in the E420A mutant. Second, Q400LfsX7 did not interact with RXR (Fig. 3A), while E420A could bind with RXR (Malloy et al., 2011). Third and importantly, our mutant strongly interacted with NCoR (Fig. 3C). Fourth, we demonstrated that Q400LfsX7 could interact with VDRE (Fig. 3D). These findings suggested that the dominant-negative effect of Q400LfsX7 was caused by a constitutive interaction with NCoR that may interact with VDRE to inhibit the activity of liganded wild-type-VDR. It is interesting that a similar molecular mechanism was postulated in the syndrome of resistance to thyroid hormone (RTH) caused by mutations in the TR α and β genes (*THRA* and *THRB*, respectively) (Safer et al., 1998; Liu et al., 1998; Fozzatti et al., 2011, 2013; Bochukova et al., 2012). In contrast to HVDRR, RTH is usually an autosomal dominant disease. This dominant inheritance had been attributed to the dominant-negative effect of mutant *THRA* or *THRB* by failing to dissociate with NCoR (Safer et al., 1998; Fozzatti et al., 2011; Bochukova et al., 2012; Refetoff et al., 1993; Jameson, 1994). Most interestingly, the THRA E403X mutant lacks helix H12 and has similarly enhanced corepressor interaction and absent ligand binding through its loss of amino acids critical for hormone binding and coactivator recruitment, as shown by crystallographic modeling (Bochukova et al., 2012). We speculated that Q400LfsX7-VDR also caused an inability to release a corepressor by exposing a hydrophobic cleft on the receptor surface through the loss of helix H12. These findings suggested that HVDRR may be inherited as a dominant trait if the mutant has a constitutive corepressor interaction causing a dominant-negative effect, similar to RTH defects.

It is notable that our patient did not have alopecia. Cumulative data indicate that functional VDR is required for hair growth, and that alopecia is unrelated to the calcium or metabolic abnormalities that cause

rickets (Malloy and Feldman, 2011). In addition, previous data indicate that VDR mutations cause defects in DNA binding, and that RXR heterodimerization or the absence of VDR causes alopecia, and mutations that alter VDR affinity for $1,25(OH)_2D_3$ or disrupt coactivator interactions do not cause alopecia (Malloy and Feldman, 2011). Our finding suggested that, although Q400LfsX7-VDR did not interact with RXR, the mutant did not affect its dominant-negative effect on wild-type-VDR for the regulation of the hair cycle. A possible explanation is that Q400LfsX7-VDR may not be overexpressed compared with wild-type-VDR in the hair follicle. Further research using this mutant is necessary to elucidate the role of VDR in hair growth and differentiation.

Our results suggested that some patients with vitamin D-deficient rickets may have a *VDR* mutation. Our patient had obvious rickets and short stature but did not have hypocalcemia. His symptoms were relatively mild when compared with the classic clinical pattern of HVDRR, and his clinical course that the medication could be stopped by 4 years of age was similar to that of vitamin D-deficient rickets. In fact, his father was treated with vitamin D under the misdiagnosis of vitamin D-deficient rickets. In addition, aside from bowlegs, his unexamined paternal grandfather was otherwise asymptomatic without medication. The resolution of vitamin D resistance in patients with HVDRR has been previously described, but it typically occurs around puberty (Tiosano et al., 2011). We consider that mild cases of HVDRR may be misdiagnosed as vitamin D deficiency or remain undiagnosed. Our results expand the concept of HVDRR and enrich our understanding of VDR function in the pathogenesis of HVDRR.

5. Conclusion

We identified a novel *VDR* mutation (Q400LfsX7) with a dominant-negative effect on wild-type VDR in a family with dominantly inherited HVDRR, and we clarified that the mutant interacted strongly with NCoR. These findings suggested a distinct inheritance of HVDRR that expanded our understanding of the condition. Further investigations and pedigree analyses are needed to reveal the mechanism underlying dominantly inherited HVDRR.

Disclosure statement

The authors declare no conflicts of interest.

Acknowledgments

We are grateful to Dr S. Kato for providing the plasmids, and Minako Takaki and Reiko Onai for their technical support. This study was supported by Grant-in-Aid from the Ministry of Education, Science, Sports, and Culture of Japan (23591489).

References

Adachi, R., Shulman, A.I., Yamamoto, K., Shimomura, I., Yamada, S., Mangelsdorf, D.J., Makishima, M., 2004. Structural determinants for vitamin D receptor response to endocrine and xenobiotic signals. Mol. Endocrinol. 18, 43–52.

Adachi, R., Honma, Y., Masuno, H., Kawana, K., Shimomura, I., Yamada, S., Makishima, M., 2005. Selective activation of vitamin D receptor by lithocholic acid acetate, a bile acid derivative. J. Lipid Res. 46, 46–57.

Bochukova, E., Schoenmakers, N., Agostini, M., Schoenmakers, E., Rajanayagam, O., Keogh, J.M., Henning, E., Reinemund, J., Gevers, E., Sarri, M., Downes, K., Offiah, A., Albanese, A., Halsall, D., Schwabe, J.W., Bain, M., Lindley, K., Muntoni, F., Vargha-Khadem, F., Khadem, F.V., Dattani, M., Farooqi, I.S., Gurnell, M., Chatterjee, K., 2012. A mutation in the thyroid hormone receptor alpha gene. N. Engl. J. Med. 366, 243–249.

Endo-Umeda, K., Uno, S., Fujimori, K., Naito, Y., Saito, K., Yamagishi, K., Jeong, Y., Miyachi, H., Tokiwa, H., Yamada, S., Makishima, M., 2012. Differential expression and function of alternative splicing variants of human liver X receptor α. Mol. Pharmacol. 81, 800–810.

Feldman, D., Malloy, P.J., 2014. Mutations in the vitamin D receptor and hereditary vitamin D-resistant rickets. Bonekey Rep. 3, 510.

Fozzatti, L., Lu, C., Kim, D.W., Park, J.W., Astapova, I., Gavrilova, O., Willingham, M.C., Hollenberg, A.N., Cheng, S.Y., 2011. Resistance to thyroid hormone is modulated in vivo by the nuclear receptor corepressor (NCOR1). Proc. Natl. Acad. Sci. U. S. A. 108, 17462–17467.

Fozzatti, L., Kim, D.W., Park, J.W., Willingham, M.C., Hollenberg, A.N., Cheng, S.Y., 2013. Nuclear receptor corepressor (NCOR1) regulates in vivo actions of a mutated thyroid hormone receptor α. Proc. Natl. Acad. Sci. U. S. A. 110, 7850–7855.

Haussler, M.R., Whitfield, G.K., Haussler, C.A., Hsieh, J.C., Thompson, P.D., Selznick, S.H., Dominguez, C.E., Jurutka, P.W., 1998. The nuclear vitamin D receptor: biological and molecular regulatory properties revealed. J. Bone Miner. Res. 13, 325–349.

Haussler, M.R., Whitfield, G.K., Kaneko, I., Haussler, C.A., Hsieh, D., Hsieh, J.C., Jurutka, P.W., 2013. Molecular mechanisms of vitamin D action. Calcif. Tissue Int. 92, 77–98.

Igarashi, M., Yoshimoto, N., Yamamoto, K., Shimizu, M., Ishizawa, M., Makishima, M., DeLuca, H.F., Yamada, S., 2007. Identification of a highly potent vitamin D receptor antagonist: (25S)-26-adamantyl-25-hydroxy-2-methylene-22,23-didehydro-19,27-dinor-20-epi-vitamin D3 (ADMI3). Arch. Biochem. Biophys. 460, 240–253.

Inaba, Y., Yamamoto, K., Yoshimoto, N., Matsunawa, M., Uno, S., Yamada, S., Makishima, M., 2007. Vitamin D3 derivatives with adamantane or lactone ring side chains are cell type-selective vitamin D receptor modulators. Mol. Pharmacol. 71, 1298–1311.

Jameson, J.L., 1994. Mechanisms by which thyroid hormone receptor mutations cause clinical syndromes of resistance to thyroid hormone. Thyroid 4, 485–492.

Jurutka, P.W., Remus, L.S., Whitfield, G.K., Thompson, P.D., Hsieh, J.C., Zitzer, H., Tavakkoli, P., Galligan, M.A., Dang, H.T., Haussler, C.A., Haussler, M.R., 2000. The polymorphic N terminus in human vitamin D receptor isoforms influences transcriptional activity by modulating interaction with transcription factor IIB. Mol. Endocrinol. 14, 401–420.

Kitanaka, S., Takeyama, K., Murayama, A., Sato, T., Okumura, K., Nogami, M., Hasegawa, Y., Niimi, H., Yanagisawa, J., Tanaka, T., Kato, S., 1998. Inactivating mutations in the 25-hydroxyvitamin D3 1alpha-hydroxylase gene in patients with pseudovitamin D-deficiency rickets. N. Engl. J. Med. 338, 653–661.

Liu, Y., Takeshita, A., Misiti, S., Chin, W.W., Yen, P.M., 1998. Lack of coactivator interaction can be a mechanism for dominant negative activity by mutant thyroid hormone receptors. Endocrinology 139, 4197–4204.

Makishima, M., Lu, T.T., Xie, W., Whitfield, G.K., Domoto, H., Evans, R.M., Haussler, M.R., Mangelsdorf, D.J., 2002. Vitamin D receptor as an intestinal bile acid sensor. Science 296, 1313–1316.

Malloy, P.J., Feldman, D., 2010. Genetic disorders and defects in vitamin D action. Endocrinol. Metab. Clin. N. Am. 39, 333–346 (table of contents).

Malloy, P.J., Feldman, D., 2011. The role of vitamin D receptor mutations in the development of alopecia. Mol. Cell. Endocrinol. 347, 90–96.

Malloy, P.J., Zhu, W., Bouillon, R., Feldman, D., 2002. A novel nonsense mutation in the ligand binding domain of the vitamin D receptor causes hereditary 1,25-dihydroxyvitamin D-resistant rickets. Mol. Genet. Metab. 77, 314–318.

Malloy, P.J., Xu, R., Peng, L., Peleg, S., Al-Ashwal, A., Feldman, D., 2004. Hereditary 1,25-dihydroxyvitamin D resistant rickets due to a mutation causing multiple defects in vitamin D receptor function. Endocrinology 145, 5106–5114.

Malloy, P.J., Zhou, Y., Wang, J., Hiort, O., Feldman, D., 2011. Hereditary vitamin D-resistant rickets (HVDRR) owing to a heterozygous mutation in the vitamin D receptor. J. Bone Miner. Res. 26, 2710–2718.

Malloy, P.J., Tasic, V., Taha, D., Tütüncüler, F., Ying, G.S., Yin, L.K., Wang, J., Feldman, D., 2014. Vitamin D receptor mutations in patients with hereditary 1,25-dihydroxyvitamin D-resistant rickets. Mol. Genet. Metab. 111, 33–40.

Nakajima, S., Hsieh, J.C., MacDonald, P.N., Galligan, M.A., Haussler, C.A., Whitfield, G.K., Haussler, M.R., 1994. The C-terminal region of the vitamin D receptor is essential to form a complex with a receptor auxiliary factor required for high affinity binding to the vitamin D-responsive element. Mol. Endocrinol. 8, 159–172.

Nakano, H., Matsunawa, M., Yasui, A., Adachi, R., Kawana, K., Shimomura, I., Makishima, M., 2005. Enhancement of ligand-dependent vitamin D receptor transactivation by the cardiotonic steroid bufalin. Biochem. Pharmacol. 70, 1479–1486.

Rachez, C., Freedman, L.P., 2000. Mechanisms of gene regulation by vitamin D(3) receptor: a network of coactivator interactions. Gene 246, 9–21.

Refetoff, S., Weiss, R.E., Usala, S.J., 1993. The syndromes of resistance to thyroid hormone. Endocr. Rev. 14, 348–399.

Rochel, N., Wurtz, J.M., Mitschler, A., Klaholz, B., Moras, D., 2000. The crystal structure of the nuclear receptor for vitamin D bound to its natural ligand. Mol. Cell 5, 173–179.

Safer, J.D., Cohen, R.N., Hollenberg, A.N., Wondisford, F.E., 1998. Defective release of corepressor by hinge mutants of the thyroid hormone receptor found in patients with resistance to thyroid hormone. J. Biol. Chem. 273, 30175–30182.

Sato, U., Kitanaka, S., Sekine, T., Takahashi, S., Ashida, A., Igarashi, T., 2005. Functional characterization of LMX1B mutations associated with nail–patella syndrome. Pediatr. Res. 57, 783–788.

Solomon, C., Macoritto, M., Gao, X.L., White, J.H., Kremer, R., 2001. The unique tryptophan residue of the vitamin D receptor is critical for ligand binding and transcriptional activation. J. Bone Miner. Res. 16, 39–45.

Tiosano, D., Hadad, S., Chen, Z., Nemirovsky, A., Gepstein, V., Militianu, D., Weisman, Y., Abrams, S.A., 2011. Calcium absorption, kinetics, bone density, and bone structure in patients with hereditary vitamin D-resistant rickets. J. Clin. Endocrinol. Metab. 96, 3701–3709.

PLOS | ONE

RESEARCH ARTICLE

Detection of Hereditary 1,25-Hydroxyvitamin D-Resistant Rickets Caused by Uniparental Disomy of Chromosome 12 Using Genome-Wide Single Nucleotide Polymorphism Array

Mayuko Tamura[1], Tsuyoshi Isojima[1], Minae Kawashima[2], Hideki Yoshida[3], Keiko Yamamoto[4], Taichi Kitaoka[4], Noriyuki Namba[4], Akira Oka[1], Keiichi Ozono[4], Katsushi Tokunaga[2], Sachiko Kitanaka[1]*

1 Department of Pediatrics, Graduate School of Medicine, The University of Tokyo, Tokyo, Japan,
2 Department of Human Genetics, Graduate School of Medicine, The University of Tokyo, Tokyo, Japan,
3 Department of Pediatrics, North Medical Center, Kyoto Prefectural University of Medicine, Kyoto, Japan,
4 Department of Pediatrics, Osaka University Graduate School of Medicine, Osaka, Japan

* sachi-tky@umin.ac.jp

OPEN ACCESS

Citation: Tamura M, Isojima T, Kawashima M, Yoshida H, Yamamoto K, Kitaoka T, et al. (2015) Detection of Hereditary 1,25-Hydroxyvitamin D-Resistant Rickets Caused by Uniparental Disomy of Chromosome 12 Using Genome-Wide Single Nucleotide Polymorphism Array. PLoS ONE 10(7): e0131157. doi:10.1371/journal.pone.0131157

Editor: Klaus Brusgaard, Odense University Hospital, DENMARK

Received: January 31, 2015

Accepted: May 31, 2015

Published: July 8, 2015

Data Availability Statement: All relevant data except for SNP array data are within the paper and its Supporting Information files. Although we could not obtain informed consent for depositing SNP array data, the de-identified participant-level dataset is available upon request to corresponding authors, and with an appropriate approval of human genomic DNA research ethics committee of institutions to which researchers involved in the data analyses belong. A minimized, anonymous dataset can be provided on request to any researcher.

Abstract

Context

Hereditary 1,25-dihydroxyvitamin D-resistant rickets (HVDRR) is an autosomal recessive disease caused by biallelic mutations in the vitamin D receptor (VDR) gene. No patients have been reported with uniparental disomy (UPD).

Objective

Using genome-wide single nucleotide polymorphism (SNP) array to confirm whether HVDRR was caused by UPD of chromosome 12.

Materials and Methods

A 2-year-old girl with alopecia and short stature and without any family history of consanguinity was diagnosed with HVDRR by typical laboratory data findings and clinical features of rickets. Sequence analysis of *VDR* was performed, and the origin of the homozygous mutation was investigated by target SNP sequencing, short tandem repeat analysis, and genome-wide SNP array.

Results

The patient had a homozygous p.Arg73Ter nonsense mutation. Her mother was heterozygous for the mutation, but her father was negative. We excluded gross deletion of the father's allele or paternal discordance. Genome-wide SNP array of the family (the patient and her parents) showed complete maternal isodisomy of chromosome 12. She was successfully treated with high-dose oral calcium.

Funding: This study was supported by Grants-in-Aid for Scientific Research from Japan Society for the Promotion of Science (to T.I. and S.K., grant number 23591489), and for Research on Intractable Diseases from the Ministry of Health, Labor and welfare (to K. O.). The funders had no role in study design, data collection and analysis, decision to publish, or preparation of the manuscript.

Competing Interests: The authors have declared that no competing interests exist.

Conclusions

This is the first report of HVDRR caused by UPD, and the third case of complete UPD of chromosome 12, in the published literature. Genome-wide SNP array was useful for detecting isodisomy and the parental origin of the allele. Comprehensive examination of the homozygous state is essential for accurate genetic counseling of recurrence risk and appropriate monitoring for other chromosome 12 related disorders. Furthermore, oral calcium therapy was effective as an initial treatment for rickets in this instance.

Introduction

Hereditary 1,25-dihydroxyvitamin D (1,25$[OH]_2$D)-resistant rickets (HVDRR) (OMIM #277440), also known as vitamin D-dependent rickets type 2A (VDDR 2A), is a rare disorder characterized by early onset rickets, hypocalcemia, and secondary hyperparathyroidism, and alopecia when severe [1]. Patients with HVDRR have high circulating levels of 1,25$(OH)_2$D, and are resistant to 1,25$(OH)_2D_3$ and 1α$(OH)D_3$ treatment. Elevated 1,25$(OH)_2$D levels differentiate HVDRR from 1α-hydroxylase deficiency, which is known as vitamin D-dependent rickets type 1A [2].

HVDRR is caused by mutations in the vitamin D receptor (VDR) gene on chromosome 12q13.11 [3]. HVDRR shows autosomal-recessive inheritance and the patients usually have biallelic mutations in the *VDR* inherited from each parent. Because of the rarity of the disease, most cases arise in consanguineous families and have homozygous mutations [4]. VDR is a member of the steroid/nuclear receptor superfamily of ligand-activated transcription factors, and it is composed of an N-terminal DNA binding domain (DBD) and a C-terminal ligand-binding domain (LBD) [5]. Patients with a mutation in the DBD usually show severe vitamin D resistance associated with alopecia [6], whereas those with a mutation in the LBD show various degrees of vitamin D unresponsiveness and can occasionally respond to high-dose vitamin D. Patients with alopecia showing resistance to high-dose vitamin D therapy usually require intravenous calcium infusions to treat clinically overt rickets at their first presentation [6].

Some recessive disorders have been reported to be caused by uniparental disomy (UPD) of a single parent allele with a mutation [7]. UPD refers to a condition in which both homologues of a chromosomal region or segment are inherited from only one parent. To date, most cases of UPD have been found in imprinting diseases such as Prader-Willi syndrome, and the incidence of UPD of any chromosome is estimated to be as frequent as 1 per 3,500 live births [8,9]. Conversely, UPD causing recessive diseases have only been reported in a limited number of cases. Moreover, no cases have been reported in HVDRR and complete isodisomy of chromosome 12 is extremely rare [7,10,11].

In this report, we used genome-wide single nucleotide polymorphism (SNP) array analysis to determine whether HVDRR was caused by UPD of chromosome 12. Furthermore, we observed the effectiveness of high oral calcium therapy for the treatment of rickets in this severe HVDRR patient.

Materials and Methods

Clinical case

A 2-year 1-month-old girl presented to hospital with fever, at which point she was noted to have short stature, alopecia (Fig 1), and gait instability. Her parents were non-consanguineous

Fig 1. Alopecia and Rickets in the Proband at Presentation. (A) Alopecia. (B,C) A bone roentgenogram of the arm (B) and legs (C) showing cupping, fraying, and flaring at the end of the long bones.

doi:10.1371/journal.pone.0131157.g001

and approximately 30 years old when she was born. She had no family history of rickets or unresolved pain. Her mother got a natural conception, and the pregnancy and delivery was uneventful. Her birth weight was 2,868 g (-0.8 standard deviations [SD]), birth length 51 cm (+0.6 SD), gestational age 41 weeks. She had no episode of convulsion and her psychomotor development was normal until she started walking alone at 1 year 3 months of age, but she could not run by age 2. Her body height at presentation was 74.8 cm (−3.5 SD), and her body weight, 9.7 kg (−1.2 SD). She had symptoms of rickets such as bow-legs and enlargement of the limb joints, but had no other external malformation, dysmorphic features, or ataxia. Her verbal developmental quotient (DQ) was 81 and cognitive DQ 94.

Laboratory data revealed hypocalcemia (7.7; reference: 8.5–10.5 mg/dL), hypophosphatemia (3.0; reference: 4.5–6.5 mg/dL), markedly elevated levels of serum alkaline phosphatase (8,891; reference: 300–1,239 IU/L), and intact parathyroid hormone (PTH) levels (576; reference: 10 −65 pg/mL). Her serum $1,25(OH)_2D$ level was high (137; reference: 20–70 pg/mL) with a normal 25(OH)D level (20.1 ng/mL). Serum levels of fibroblast growth factor 23 (FGF23) were

low (<10 pg/mL), and a bone roentgenogram showed characteristic findings of rickets (Fig 1). From these findings, she was clinically diagnosed as having HVDRR.

VDR gene analysis

We obtained written informed consent for DNA analysis from the parents, and the Ethics Committee of The University of Tokyo approved the study. Genomic DNA was extracted from peripheral white blood cells of the patient and parents using a QIAamp DNA Blood Midi Kit (Qiagen, Hilden, Germany). The entire coding region and exon-intron boundaries of the *VDR* were amplified from the genomic DNA by polymerase chain reaction (PCR) using the specific primers (S1 Table). PCR products were subsequently sequenced using an ABI Prism BigDye Terminator Cycle Sequencing Ready Reaction Kit (PE Applied Biosystems, Foster City, CA) and the forward and reverse primers from the PCR amplification. Direct sequencing in both directions was performed on an autosequencer (PE Applied Biosystems 3130x1, Genetic Analyzer).

Analysis of common gene polymorphisms

Common SNPs in the *VDR* (rs10735810, rs7975232, rs2853562 rs731236, rs12717991), other genes on chromosome 12 (rs2259820, rs2464196, rs1169289, rs1169288, rs1169301, rs1169304, rs10877012), and other chromosomes (rs4588, rs7041, rs116930, rs1155563, rs2060793, rs3829251, rs6013897, rs6599638, rs10741657, rs12785878, rs17217199) were analyzed by sequencing the PCR products as previously reported [12,13]. Short tandem repeat (STR) analysis was performed using AmpFLSTR Identifiler kit (Identifiler, Applied Biosytems, Foster City, CA, USA), which included 16 STR markers (D8S1179, D21S11, D7S820, CSF1PO, D3S1358, TH01, D13S317, D16S539, D2S1338, D19S433, vWA, TPOX, D18S51, Amelogenin, D5S818, and FGA), according to the manufacturer's protocol.

Genome-wide SNP array

Using of the Affymetrix Axiom ASI 1 array (Affymetrix, CA, USA) in accordance with the manufacturer's instructions, we genotyped a total of 600,307 SNPs for the three individuals. Genotype calls were determined using the Genotyping Console 4.1.4 software with the Birdseed v2 algorithm provided by the manufacture. In addition to data from the patient and her parents, we also used 474 Japanese individuals to ensure reliable genotype calling. Signal intensities for alleles A and B were observed by using Affymetrix Power Tools [14]. B allele frequency was calculated by using of the intensities of both alleles: BAF = B / (A + B).

Results

Identification of the *VDR* mutation

Sequencing the *VDR* in the patient revealed a single homozygous base pair substitution, c.217C>A (Fig 2A). This substitution was predicted to result in a nonsense mutation p.Arg73-Ter, which is a premature stop codon in the DBD (Fig 2B). This mutation has been reported in 5 other patients with HVDRR and is functionally inactive [15–18]. From these findings, we considered that HVDRR in this patient was caused by a homozygous nonsense mutation in the *VDR*.

Analysis of the genesis of homozygosity

Most cases of homozygosity among rare mutations are caused by consanguinity, but the parents in this case denied consanguinity; therefore, we performed a genetic analysis of the parents. The mutation was heterozygous in the mother only, and was not present in the father (Fig 2A).

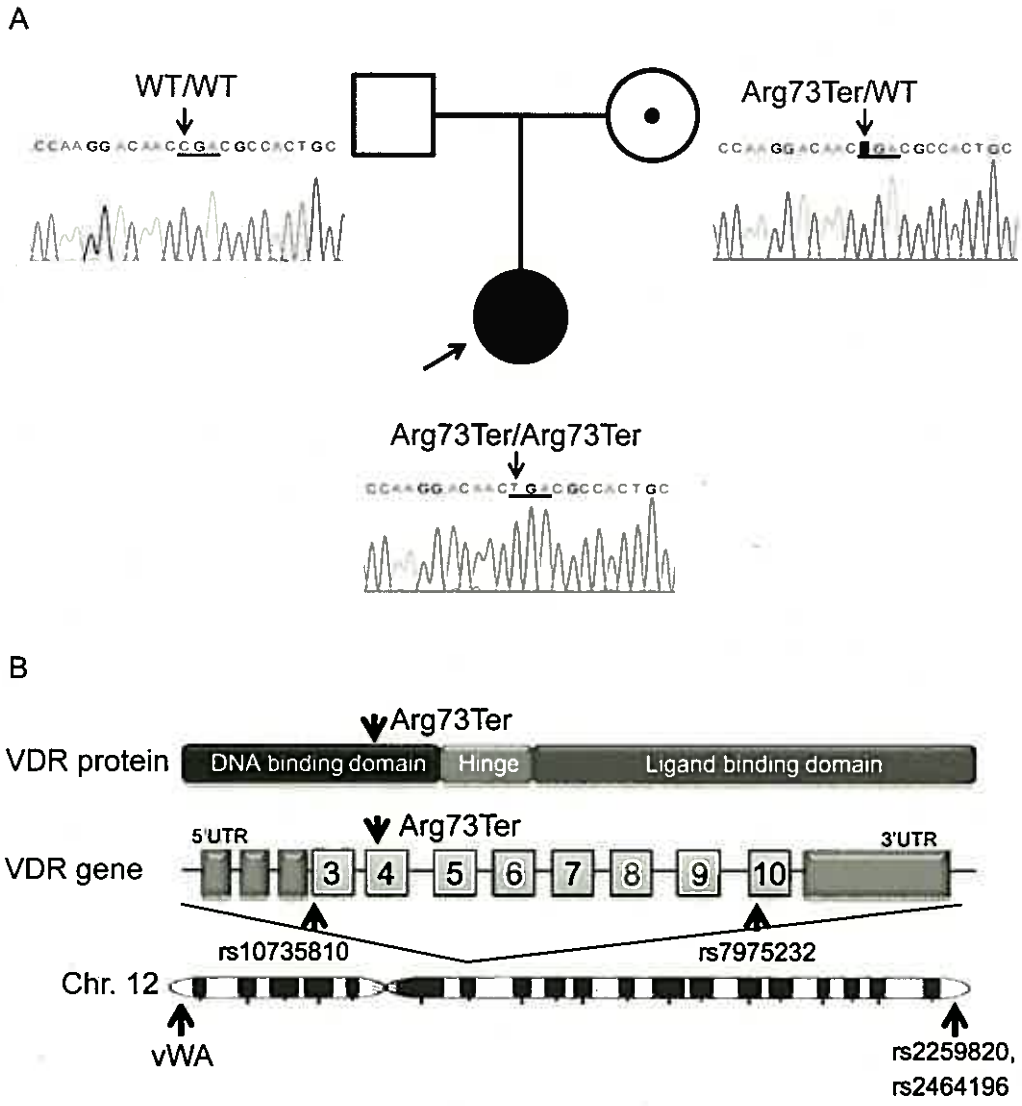

Fig 2. *VDR* Analysis of the Proband and her Parents, with the Position of the Target SNPs on Chromosome 12. (A) Proband pedigree with chromatograms of the *VDR* mutation. The *VDR* analysis showed a homozygous Arg73Ter mutation in the proband, a heterozygous mutation in the mother, and no mutation in the father. Mutations were checked by bidirectional sequencing. A black symbol indicates the proband, a dot symbol indicates a carrier, a square indicates a male, and a circle indicates a female. (B) Diagram of the VDR protein and gene, and chromosome 12 with positions of the mutation and the sequence-analyzed SNPs. The nonsense mutation, Arg73Ter, is located in the DNA binding domain of the VDR protein in exon 4. The indicated common SNPs were analyzed in the family; vWA indicates the position of a marker included in the STR analysis.

doi:10.1371/journal.pone.0131157.g002

To assess the possibility of a gross deletion around the mutation in the father's allele, we sequence-analyzed several common target SNPs in the *VDR*, in other genes on chromosome 12, and in other chromosomes studied in our laboratory. Table 1 shows the results of the SNPs which identify the parental origin of the proband's allele. Two SNPs in the *VDR*, one near the mutation (rs10735810) and another within approximately 20 kb (rs7975232) (Fig 2B), demonstrated homozygous alleles in the proband that were derived only from the mother (Table 1). Moreover, another 2 SNPs located at the opposite end of the long arm of chromosome 12

Table 1. Sequence Analysis of the Common Target SNPs that Could Identify Parental Origin.

Gene	SNP	Location	Proband	Father	Mother
VDR	rs10735810	12q13.11	CC	TT	CT
VDR	rs7975232	12q13.11	GG	TT	GG
HNF1A	rs2259820	12q24.31	CC	TT	CC
HNF1A	rs2464196	12q24.31	GG	AA	GG
NADSYN1	rs3829251	11q13.4	GA	GG	AA
GC	rs7041	4q13.3	TG	TG	GG
GC	rs1155563	4q13.3	CT	CC	TT

doi:10.1371/journal.pone.0131157.t001

(rs2259820, rs2464196) (Fig 2B) were also homozygous and derived only from the mother. However, SNPs on chromosomes 4 and 11 showed a normal pattern of allele inheritance from the parents. These results indicated that at least the long arm of chromosome 12 consists of alleles derived only from the mother. G-banding karyotype analysis of the proband revealed a normal 46,XX karyotype without monosomy of 12q. These findings suggested that gross deletion of the father's allele was unlikely.

Next, we assessed the biological paternity by conventional STR analysis. STRs located on chromosomes other than 12 confirmed that the father was the biological father. Interestingly, the STR of a gene located on the short arm of chromosome 12 (vWA; 12p12-pter) showed a homozygous maternal allele (proband 19; father 14, 16; mother 16, 19). Taken together, these findings eliminated the possibility of a gross deletion and paternal discordance, and suggested that *de novo* mutation was unlikely. Finally, maternal UPD of the entire chromosome 12 was suggested.

Detection of UPD by genome-wide SNP array

For the evaluation of UPD, we conducted a genome-wide SNP array of the proband and the parents. The overall call rates were 99.47%, 99.64%, and 99.57% for the proband, the father, and the mother, respectively. All chromosomes other than chromosome 12 showed a normal homo/heterozygous pattern. There were 29,197 SNPs on chromosome 12 on the array, of which 13,940 SNPs showed multiple genotypes among the trio of samples (proband, mother, and father). The proband was called homozygous for 13,848 SNPs and heterozygous for 92 SNPs; however, we found that these heterozygous SNPs were miss-calls caused by the genotype calling algorithms, and the proband was considered homozygous for all SNPs on chromosome 12. After linkage disequilibrium pruning (LD pruning) with 474 samples, a total of 8,933 SNPs remained [19,20], except for bad clusters. Fig 3 shows the B allele frequencies for chromosome 12, which represents the distribution of each proband, maternal, and paternal allele. On chromosome 12, the allele segregation revealed to be composed of only homozygous AA and BB combinations, and no AB combinations (loss of heterozygosity). Allele segregation of chromosome 12 showed a heterozygous pattern in her parents. In the proband's diagram, the pink spots represent the maternal SNPs (1,514 SNPs) and the blue spots, paternal (none) (Fig 3). It was obvious that all of the homozygous SNPs on chromosome 12 derived from the mother. Moreover, the 2 alleles in the proband were 100% identical to those in the mother by identical-by-descent analysis, whereas none were identical to those in the father [21]. The signal intensity of chromosome 12 was sufficient to conclude that the chromosome was diploid, compared with other chromosomes. Thus, we concluded that the proband had complete maternal uniparental isodisomy of chromosome 12 with a nonsense mutation.